JOURNAL OF APPLIED PHYSICS VOLUME 88, NUMBER 6 15 SEPTEMBER 2000

The electro-optic properties of interdiffused InGaAs/InP quantum well structures

Bernard L. Weiss
Department of Electronic & Electrical Engineering, University of Surrey, Guildford, Surrey GU2 5XH, United Kingdom

Y. Chan
Department of Electrical and Electronic Engineering, University of Hong Kong, Pokfulam Road, Hong Kong

W. C. Shiu
Department of Mathematics, Hong Kong Baptist University, Waterloo Road, Hong Kong

E. Herbert Li[a)]
Department of Electrical and Electronic Engineering, University of Hong Kong, Pokfulam Road, Hong Kong

(Received 1 July 1999; accepted for publication 21 January 2000)

We present a model for the optical properties of interdiffused InGaAs/InP quantum well structures. The structure is investigated in a two-phase group V interdiffusion that is characterized by three parameters: the interdiffusion coefficient in the barrier layer, the well layer, and the concentration ratio of diffused species at the well/barrier interface. The quantum confined Stark effect is considered including the exciton and full subband under an applied electric field. Results show interesting optical properties for the TE and TM polarization and a tunable operation wavelength near 1.55 μm for modulators. © *2000 American Institute of Physics.* [S0021-8979(00)00609-5]

I. INTRODUCTION

InGaAs/InP quantum well (QW) structures have being investigated for a variety of optoelectronic devices, such as modulators,[1] detectors,[2] waveguides,[3] and lasers[4] at 1.3–1.55 μm wavelengths. Recent improvements in metalorganic vapor phase epitaxy[5] and molecular beam epitaxy[6] have enabled high-quality InGaAs/InP strained-layer structures to be fabricated. There is a growing interest in selective area disordering of these QW structures[7] using masked ion implantation[8] and masked impurity diffusion,[9] with special emphasis on high-performance device applications and monolithic integration. The disordering process involves thermally induced interdiffusion of the constituent atoms across the well/barrier interface, where the rate of the interdiffusion process is a function of the nature and dose (concentration) of the implanted (impurity) ions, also the annealing temperature and time. The interdiffusion process modifies the compositional profile of the as-grown square QW to produce a graded profile, known as diffused QW (DFQW), which modifies the electronic and optical properties of the QW structure. This interdiffusion process provides a useful tool for the controlled localized band gap engineering, which is required for the development of optoelectronic devices and integrated circuits.[10]

QW devices are important for the next-generation of optoelectronic systems and the properties of these devices are strongly dependent on their subband structure. Thermal interdiffusion can modify the structure of the QW, which changes band gap energy of the QW structure. Thermal interdiffusion occurs at temperatures above 800 °C in $GaAs/Al_xGa_{1-x}As$ QW structures[11] and above 500 °C in $In_{0.53}Ga_{0.47}As/InP$ QW structures.[12] In InGaAs/InP QW structures, the interdiffusion mechanisms are more complex since interdiffusion can occur for both group III (In, Ga) and group V (As, P) atoms. It is precisely this possibility which enables interdiffusion to both increase and decrease the QW band gap depending on whether the group III or group V atoms are moving. It is extremely important to understand this interdiffusion mechanism. The confinement profile of interdiffused $GaAs/Al_xGa_{1-x}As$ single QW has been described by an equation having a smooth symmetric profile.[13] Nevertheless, the interdiffusion processes in $In_{0.53}Ga_{0.47}As/InP$ QW is not fully understood. Recently, three types of interdiffusion models have been studied: (i) group III and group V interdiffusion, which produces either a compressive or tensile strained QW; (ii) group III interdiffusion, which only produces a compressive strained well layer and a tensile barrier layers, and (iii) group V interdiffusion, which is only governed by a two phase interdiffusion process where the well is under tensile strain while the barrier is compressively strained. Nakashima *et al.*[14] reported that the main interdiffusion species in $In_{0.53}Ga_{0.47}As/InP$ QW structures annealed at 700 °C are group V atoms, as shown by x-ray analysis, while Temkin *et al.*[15] reported that transmission electron microscopy could not detect a graded layer at the well/barrier interface after interdiffusion. Yet, a qualitative investigation of the quantum confinement energies by Fuji *et al.*[12] suggested that the concentration of group V atoms was discontinuous at the interface while Mukai *et al.*[16] proposed a two-

a)Author to whom correspondence should be addressed; electronic mail: ehli@eee.hku.hk

phase diffusion model that is supported by experimental evidence. Subsequently a model has been developed using a time dependent diffusivity.[17]

The interband electroabsorption near the band edge of the QW structure has received considerable attention for modulator applications. QW structures have a much larger change in electroabsorption than bulk GaAs and InP due to the quantum confined Stark effect.[18] The optical properties of DFQWs have also attracted attention for the improvement of optical device performance and optoelectronic integration.[19] Most of these studies, however, are concerned with the AlGaAs/GaAs and InGaAs/GaAs material systems. In this article, the electric field induced change in the absorption coefficient and refractive index around the exciton band edge of an InGaAs/InP single QW structure are studied theoretically as a result of group V interdiffusion only.

II. THE MODEL

The QW structure studied here consists of a single as-grown $In_{0.53}Ga_{0.47}As$ well which is clad above and below with thick lattice matched InP barrier layers and the structure is grown on an InP substrate. Interdiffusion in the DFQW is modeled, assuming different anion diffusion rates exist for the well and the barrier layers where an abrupt jump of group V element concentration is formed at the interface;[20] this process is known as a two-phase interdiffusion. The extent of interdiffusion is characterized by diffusion length L_d, which is defined here as $L_d=(Dt)^{1/2}$ (D is the diffusion coefficient and t is the annealing time). In the case of two-phase anion interdiffusion, two diffusion lengths are required on the grounds that the extent of the interdiffusion in the well and barrier layers is different; L_d^W and L_d^B are defined as the well and barriers layers, respectively. The electron and hole subbands are calculated numerically, taking into consideration the conduction band nonparabolicity and valence band mixing under an applied electric field, using the scheme developed by Bloss.[21] These subbands are then utilized to calculate the heavy-hole (HH) and light-hole (LH) related $1S$ exciton binding energies and wave functions by a perturbative-variational method.[22] In terms of an optical waveguide structure, for light propagating in the plane of the QW layers the TE and TM polarizations have their E field vectors perpendicular and parallel to the QW growth axis, respectively. The external electric field is applied perpendicular to the QW layers, as in a *p-i-n* structure.

A. Two-phase group V interdiffusion

Annealing $In_xGa_{1-x}As$/InP QW structures produces interdiffusion across the well/barrier interface due to the difference of concentration gradients. It has been reported that interdiffusion in GaAs/$Al_xGa_{1-x}As$ occurs above 800 °C,[16] while in $In_{0.53}Ga_{0.47}As$/InP it starts at ~500 °C.[16] In addition, interdiffusion is a more complex process in the $In_xGa_{1-x}As$/InP system because both group III and group V atoms can participate in the interdiffusion process.

As for the case of only group V interdiffusion, $In_xGa_{1-x}As_yP_{1-y}$ will be formed in the well and $InAs_yP_{1-y}$ in the barrier. In addition, the lattice constant of the barrier layer is greater than that of the substrate, resulting in a biaxial hydrostatic strain on the barrier layer parallel to the interfacial plane and a uniaxial shear strain perpendicular to the interfacial plane.

Secondary ion mass spectroscopy has shown that $D_{III} \approx D_V$ at higher temperatures, whereas $D_V > D_{III}$ at lower temperatures; also the rate of interdiffusion was limited by the InP barrier layers.[23]

As for a heterojunction or a QW structure, the interdiffusion process can be described by a linear diffusion equation (1). In the QW structure the InGaAs well layer is surrounded by two InP barrier layers and, if the diffusion coefficients are assumed to be different for the well and barrier layers, the diffusion equations governing this system are

$$\frac{\partial f_i(z,t)}{\partial t} = D_i \frac{\partial^2 f_i(z,t)}{\partial z}, \quad t \geqslant 0, \tag{1}$$

where f is the As concentration and D is the corresponding diffusion coefficient, $i=B$ (denotes barrier) when $|z| \geqslant L_z/2$ and $i=W$ (denotes well) when $|z| \leqslant L_z/2$.
The boundary conditions are

$$f_B(z,t) = k f_W(z,t), \quad \text{for } z \rightarrow \pm L_z/2, \tag{2}$$

$$D_B \frac{\partial f_B(z,t)}{\partial t} = D_W \frac{\partial f_W(z,t)}{\partial z}, \quad \text{for } z \rightarrow \pm L_z/2, \tag{3}$$

where f_B and f_W are the concentrations of the diffusing species (As) on each side of the well/barrier interface, and k is the concentration ratio of diffused species at the well/barrier. Equation (2) describes the discontinuity of the concentration at the interfaces and Eq. (3) describes the flux continuity.

Considering an undoped, single $In_xGa_{1-x}As$ well layer, lattice matched to semi-infinite InP barriers, it is found that the concentration of the interdiffused atoms across the QW structure, after interdiffusion, is solved using the finite difference method. In the present anion interdiffusion model, since only group V (As and P) interdiffusion exists, W is a constant and is given by $W_0=0.53$. Therefore, from the above equations the anion interdiffusion in an $In_xGa_{1-x}As$/InP QW is characterized by the two diffusion lengths, $L_d^W=\sqrt{D_W t}$ and $L_d^B=\sqrt{D_B t}$ for the well and the barrier layers, respectively. When $L_d^W=L_d^B$ the interdiffusion is one phase process.

The compositional profiles in the DFQW structure imply that the carrier effective masses, the bulk band gap, and the strain vary across the QW. Consequently, the carrier effective mass $m_r^*(z)$ is z dependent and is obtained from $m_r^*(z)=m_r^*(W_0,f)$, where $m_r^*(W_0,f)$ is the respective bulk carrier effective mass, and r denotes the electron (C), the heavy hole (V=HH) or the light hole (V=LH). The unstrained band gap in the well $E_g(W,f)$ is also a function of the compositional profile, so that after interdiffusion the unstrained potential profile $\Delta E_r(W,f)$ varies across the well and is given by

$$\Delta E_r(W_0,f) = Q_r \Delta E_g(W_0,f), \tag{4}$$

where Q_r is the band offset and ΔE_g is the unstrained band gap offset.

B. Bound states

As long as the thickness of the QW layer is within the critical layer thickness regime, the QW structure will be coherently strained after interdiffusion, with a biaxial hydrostatic strain parallel to the interfacial plane and a uniaxial shear strain perpendicular to the interfacial plane (plane of the QW). In addition, the shear strain causes the LH band to couple with the spin-orbit split-off band.

The change in the bulk band gap due to the biaxial component of strain $S_{\|}(w,f)$ is given by[24]

$$S_{\perp}(W,f)=-2a(w,f)[1-c_{12}(w,f)/c_{11}(w,f)]\epsilon(w,f), \tag{5}$$

where

$$a(w,f)=-\left\{[c_{11}(w,f)+2c_{12}(w,f)]\frac{dE_g(w,f)}{dP}\right\}\Big/ 3$$

and $c_{1j}(w,f)(j=1,2)$ are the elastic stiffness constants, where $dE_g(w,f)/dP$ is the hydrostatic pressure coefficient of the lowest direct energy gap E_g. The splitting energy, $S_{\|}(w,f)$, between the HH and LH band edges induced by the uniaxial component of strain is given by

$$S_{\|}(w,f)=-b(w,f)[1+2c_{12}(w,f)/c_{11}(w,f)]\epsilon(w,f), \tag{6}$$

where $b(w,f)$ is the shear deformation potential. The coupling between the LH and the splitoff band gives rise to an asymmetric HH to LH splitting, so that

$$S_{\|\mathrm{HH}}(w,f)=S_{\|}(w,f), \tag{7}$$

$$S_{\|\mathrm{LH}}(w,f)=-[S_{\|}(w,f)+\Delta_0(w,f)]/2+[9\{S_{\|}(w,f)\}^2+\{\Delta_0(w,f)\}^2-2S_{\|}(w,f)\Delta_0(w,f)]^{1/2}, \tag{8}$$

where $\Delta_0(w,f)$ is the spin-orbit splitting. The confinement potential of the interdiffused QW, which is obtained by modifying the bulk postprocessing potential profile with the variable strain effects, is given by[3,5]

$$U_r(z)=Q_r[\Delta E_g(w,f)-S_{\perp_r}(w,f)]\pm S_{\|r}(w,f), \tag{9}$$

where $S_{\perp_r}(w,f)$ is the change in the bulk band gap due to the biaxial component of strain, and $S_{\|r}(w,f)$ is the potential corresponding to the HH and LH band edge splitting induced by the uniaxial component of strain. The positive and negative signs represent the confined HH and LH profile, respectively, and for the confined electrons $S_{\|r}(w,f)=0$.

This interdiffusion produces a nonsquare potential profile that alters the band gap energy and it can be applied to fine tune the band gap energy.

In the presence of an external applied field F, the profile becomes

$$U_r(z)=Q_r[\Delta E_g(w,f)-S_{\perp_r}(w,f)]\pm S_{\|r}(w,f)+zeF, \tag{10}$$

where e is the electric charge and z is the growth direction.

The subband structure at Γ (zone center) can be determined using the Schrödinger equation with the BenDaniel–Duke model[25] which applies the envelope function approximation. The one-dimensional Schrödinger equation for the interdiffused quantum wells is:

$$-\frac{\hbar^2}{2}\frac{d}{dz}\left[\frac{1}{m_r^*(z)}\frac{d\chi_{r1}(z)}{dz}\right]+U_r(z)\chi_{r1}(z)=E_{r1}\chi_{r1}(z), \tag{11}$$

where the growth direction z is the confinement axis, $\chi_{r1}(z)$ is the envelope wave function, E_{r1} is the quantized energy level, $m_r^*(z)$ is the carrier effective mass in the z direction, and $1=p$ or q refers to the quantized subband energy levels for the electron and holes respectively. This equation is solved numerically to obtain the quantized energy levels (E_{Cp},E_{Hq}) and the envelope wave functions (χ_{Cp},χ_{Hq}). Hence, both the interband transition energy levels $E_g+E_{Cp}+E_{Hq}$ between the pth conduction subband and the qth valence subband and the corresponding overlap integral $\langle\chi_{Cp}|\chi_{Vq}\rangle$ can be determined by using the wave functions as follows:

$$\langle\chi_{Cp}|\chi_{Vq}\rangle=\int_{-z_b}^{z_b}\chi_{Vq}^*(z)\chi_{Cp}(z)dz, \tag{12}$$

with $-z_b$ and z_b taken to be the boundaries where $\chi_{r1}(z_b)\rightarrow 0$.

C. Excitons

In order to account for the excitons, another Hamiltonian matrix element is added to the original matrix element. The $1S$ bound exciton wave function is determined by a perturbation–variational method.[22] To facilitate the calculation, a variational parameter λ is included, and by minimizing the following equation,[26] the envelope function is given by

$$\int\int dz_e\,dz_V|\chi_{C1}(z_e)|^2|\chi_{V1}(z_V)|^2 \times\{\tfrac{1}{4}a_B+Z-\tfrac{1}{2}\pi Z[H_1(4\lambda Z/a_B)-N_1(4\lambda Z/a_B)]\}, \tag{13}$$

where z_C and z_H represent the position of the electrons and holes, respectively, $Z=|z_C-z_H|$, χ_{C1}, χ_{H1} are the electron and hole envelope wave functions, respectively, H_1 and N_1 are the Struve and Newmann functions of the first order respectively, and $a_B=4\hbar\pi\epsilon^2/(\mu_{\|}^*e^2)$ is the exciton Bohr radius.

The $1S$ exciton envelope wave function, $\chi_{1S}(\rho)$, and the binding energy E_b are defined by

$$\chi_{1S}(\rho)=\frac{4\beta}{a_B\sqrt{2\pi}}\exp(-2\rho\beta/a_B) \tag{14}$$

and

$$E_b=-4\lambda^2R,$$

where $R=\mu_{\|}^*e^4/32\pi^2\epsilon^2\hbar^2$ is the exciton Rydberg energy and ρ is the relative distance between the electron and hole in the QW along the transverse direction, which is parallel to the QW plane and $\mu_{\|}^*=m_em_{\|}/(m_e+m_{\|})$ is the reduced mass in the transverse direction.

D. Absorption coefficient and refractive index

The TE and TM polarized absorption coefficients are considered at the Brillouin zone center Γ, including the 1*S* exciton, all bound states and the two dimensional (2D) enhanced Sommerfeld factor.

As for the bound state contribution to the absorption coefficient at the band edge Γ region of the Brillouin zone $\alpha_{od}(\omega)$ is given by

$$\alpha_{od}(\omega)=\frac{e^2\mu_{\parallel}^*\omega}{6e_0c_0n_rm_e^*E_{CV}^2L_z}M_0\sum_{p,q}|\langle\chi_{Cp}|\chi_{Vq}\rangle|^2I_{pq}(\hbar\omega), \tag{15}$$

where

$$M_0=\frac{E_g(E_g+\Delta_0)}{E_g+\frac{2}{3}\Delta_0};$$

$$I_{pq}(\hbar\omega)=\int_0^{\infty}\wp(E)S(E)L(E)dE,$$

$$S(E)=\frac{2}{1+\exp(-2\pi\sqrt{R/E})},$$

and

$$L(E)=\frac{\Gamma_B}{\pi\{[E_{CV}+E-\hbar\omega)^2+\Gamma_B^2\}},$$

where $S(E)$ is the Sommerfeld enhancement factor, $L(E)$ is the Lorentzian broadening factor, Γ_B is the bound state linewidth broadening factor (half width half maximum), $\wp(E)$ is the polarization factor, $E_{CH}(=E_g+E_{C1}+E_{H1})$, E_g is the interdiffusion induced band gap at $z=0$, c_0 is the velocity of light in free space, ε_0 is the permittivity of free space and m_c^* is the effective electron mass.

As for the light propagating along the QW growth axis there is only one polarization where the electric field vector is in the plane of the QW and the polarization factor is given by ‰=3/2(HH), 1/2 (LH). Nevertheless, for the light propagating parallel to the quantum well layer both the TE and the TM polarizations exist and there are electric field vectors both parallel and perpendicular to the plane of the quantum well. The polarization factors are given by

$$\wp^{TE}=\begin{cases}\frac{3}{4}(1+E_R) & \text{HH}\\ \frac{5}{4}(1-\frac{3}{5}E_R) & \text{LH}\end{cases}$$

$$\wp^{TM}=\begin{cases}\frac{3}{2}(1-E_R) & \text{HH}\\ \frac{1}{2}(1+3E_R) & \text{LH}\end{cases}$$

where $E_R=(E_{Cp}+E_{Hq})/(E_{Cp}+E_{Hq}+E)$.

The exciton absorption coefficient $\alpha_{1S}(\omega)$ is given by

$$\alpha_{1S}(\omega)=\frac{A\omega}{c_0n_r}|\chi(\rho=0)|^2\frac{\Gamma_{eb}}{\pi\{(E_{exc}-\hbar\omega)^2+\Gamma_{eB}^2\}}, \tag{16}$$

where

$$A=\frac{e^2\hbar^2}{2\varepsilon_0m_e^*E_{CV}^2L_z}M_0|\langle\chi_{Ci}|\chi_{Vi}\rangle|^2\wp,$$

$E_{exc}=E_{C1}+E_{H1}+E_g+E_b$ is the exciton transition energy and Γ_{eB}=exciton linewidth (half width half maximum) broadening factor. As for the 1*S* exciton only, $\rho=0$ is allowed and hence $\wp^{TE}=3/2$(HH), 1/2 (LH) and $\wp^{TM}=0$(HH), 2(LH).

The absorption coefficients α are obtained using $\alpha=\alpha_{bd}+\alpha_{1S}$ so that its changes due to an external field can be found by subtracting the value without electric field from the one with field, that is $\Delta\alpha=\alpha(F)-\alpha(F=0)$. Using the Kramers–Krönig relationship, the change in refractive index, which is determined from the change in absorption coefficient, is given by[27]

$$\Delta n(E)=\frac{c}{\pi}PV\int_0^{\infty}\frac{\Delta\alpha(E')dE'}{(E')^2-E^2}, \tag{17}$$

where E is the photon energy and PV is the principal Cauchy integral.

This model enables an effective determination of the two important optical parameters, the change of both the absorption coefficient and the refractive index with applied external field.

III. RESULTS AND DISCUSSION

A. Implementation of the model

The as-grown structure analyzed here is an $In_{0.53}Ga_{0.47}As$/InP single QW with a well width $L_z=100$ Å. The as-grown QW is assumed to be fabricated on the InP substrate with the InGaAs well layer being lattice matched to the InP barrier layers. The interdiffusion of group V anions is modeled by two-phase diffusion models which consist of three parameters—the interdiffusion coefficients of the barrier D_B and well D_W layers; and the concentration ratio of the diffused species at the well/barrier interface k. Each of these three parameters needs to be determined for each interdiffusion process to enable the model to be applied to real processes. Experimental results of the low temperature interdiffusion induced transition energy shifts for various well widths have already been reported.[20] This enables realistic low temperature interdiffusion parameters to be determined and utilized in the model.

The material parameters applied to model the QW structures are the linear interpolation between the binary parameters given in Table I. The generalized parameter T and the binary compounds *AB*, *AC*, *BC*, and *BD* can be derived from the four binary parameters using the following interpolation scheme:[28]

$$T(w,f)=(1-w)fT_{BC}+wfT_{AC}+w(1-f)T_{AD}+(1-w)(1-f)T_{BD}.$$

The conduction band offset value Q_C used here is 0.675, which is in agreement with experimental values obtained previously using optical techniques.[29] The full-width-half-maximum broadening factor is taken to be 20 meV.[30] These values have been used to determine the transition energies and the corresponding wave functions. In this model, for an annealing temperature of 650 °C, D_B is fixed at 1.9×10^{-19} cm^2/s[20] and D_W and k are varied. The calculated

TABLE I. InGaAsP material parameters at room temperature (300 K) ($m_0=9.11\times10^{-31}$ kg, $\varepsilon_0=8.85$ pF/m).

	Unit	$In_wGa_{1-w}As_fP_{1-f}$
E_g	eV	$1.35-1.17f+0.668(1-w)-0.069f(1-w)+0.18f^2+0.03(1-w)f^2+0.758(1-w)^2-0.322f(1-w)^2$
Δ_0	eV	$0.34(1-w)f+0.41wf+0.08(1-w)(1-f)+0.11w(1-f)$
m_e	m_0	$0.0632(1-w)f+0.0213wf+0.17(1-w)(1-f)+0.077w(1-f)$
m_{lh}	m_0	$0.088(1-w)f+0.024wf+0.16(1-w)(1-f)+0.12w(1-f)$
m_{hh}	m_0	$0.5(1-w)f+0.41wf+0.54(1-w)(1-f)+0.6w(1-f)$
c_{11}	$\times10^{11}$ dfn/cm^2	$11.9(1-w)f+8.329wf+14.05(1-w)(1-f)+10.11w(1-f)$
c_{12}	$\times10^{11}$ dfn/cm^2	$5.38(1-w)f+4.526wf+6.203(1-w)(1-f)+5.61w(1-f)$
a_0	Å	$5.6533(1-w)f+6.0583wf+5.4505(1-w)(1-f)+5.8687w(1-f)$
dE_g/dP	eV/bar	$11.3(1-w)f+10.2wf+10.7(1-w)(1-f)+8.4w(1-f)$
ε (static)	ε_0	$13.18(1-w)f+14.55wf+11.1(1-w)(1-f)+12.35w(1-f)$
B	eV	$-1.7(1-w)f+(-1.8)wf+(-1.8)(1-w)(1-f)+(-2.0)w(1-f)$
m_{lhll}	m_0	$0.23(1-w)f+0.082wf+0.34(1-w)(1-f)+0.29w(1-f)$
m_{hhll}	m_0	$0.11(1-w)f+0.031wf+0.19(1-w)(1-f)+0.15w(1-f)$

interdiffusion induced band gap energy shift is shown in Fig. 1 for various well widths and annealing times, which show a consistent trend corresponding to the experimental data. In the above calculation, for annealing times of 2, 6, and 8 h, D_W is taken to be 1.3×10^{-17}, 1.0×10^{-17}, and 1.2×10^{-17} cm^2/s, respectively, and k is 18, 24, and 23, respectively. In the case of the 15 h diffusion, it is assumed that they are of the same order as the values for the 8 h diffusion. These values are used in the subsequent calculation of the QW Stark effect and optical parameters.

The electro-optic effect is solved using the above parameters. The width of the quantum well is set at 14 nm because such QWs have a ground state transition energy corresponding to a wavelength of ~1.55 μm, which is of interest for optical fiber applications. The effects of annealing time and applied electric fields are considered to determine the change in absorption coefficient and refractive index.

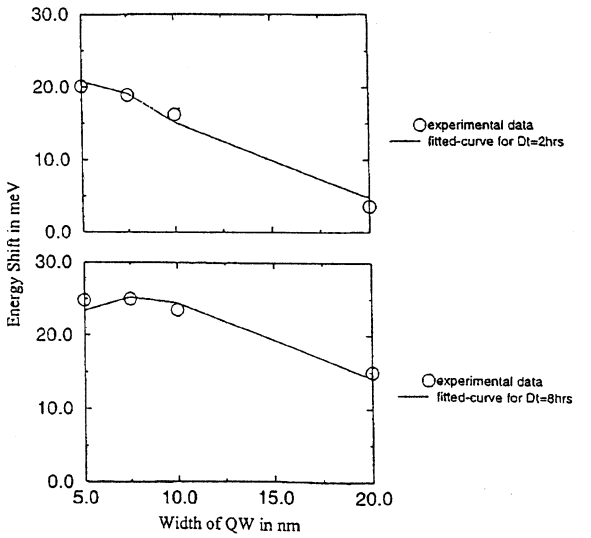

FIG. 1. QW transition energy shift as a function of well width for In0.53Ga0.47As/InP QW after annealing at 650 °C for (D_t) values of 2 and 8 h using data from Ref. 20.

B. Interdiffusion effects in quantum wells

The group V atomic profiles across the QW before and after interdiffusion are shown in Fig. 2. As the diffusion length increases, As atoms diffuse into the InP barrier and P atoms diffuse into the QW, forming an InGaAsP/InAsP interface while the Ga and In profiles are unaffected. The As and P concentration profiles in the interdiffused QW structure are determined using the finite difference method. Since the InGaAs lattice constant is always greater than that of InGaAsP, a tensile strain is produced in the QW layer near the interface. Similarly, as the lattice constant of InP is always smaller than that of InAsP, the barrier layer near the interface is compressively strained. Consequently, interdiffusion in lattice matched InGaAs/InP results in a strained QW structure.

The electron confinement profiles under the influence of an external electric field for interdiffusion lengths of 0 and 13.4 nm are shown in Fig. 3. As we can see, apart from the

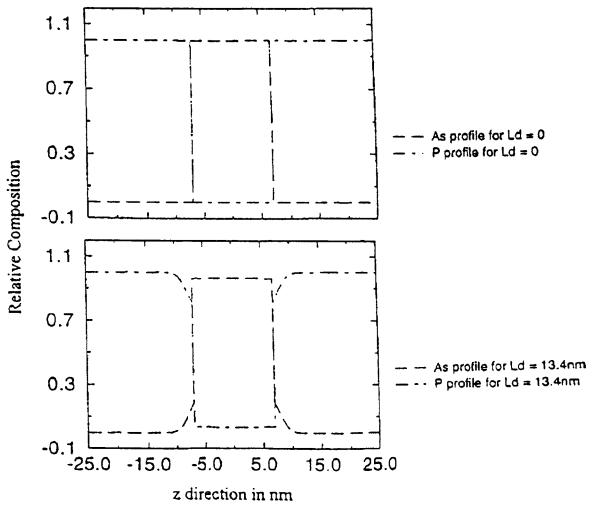

FIG. 2. The As and P compositional depth profiles across the QW for as-grown ($L_d=0$ nm) and interdiffused ($L_d=13.4$ nm) QW structures.

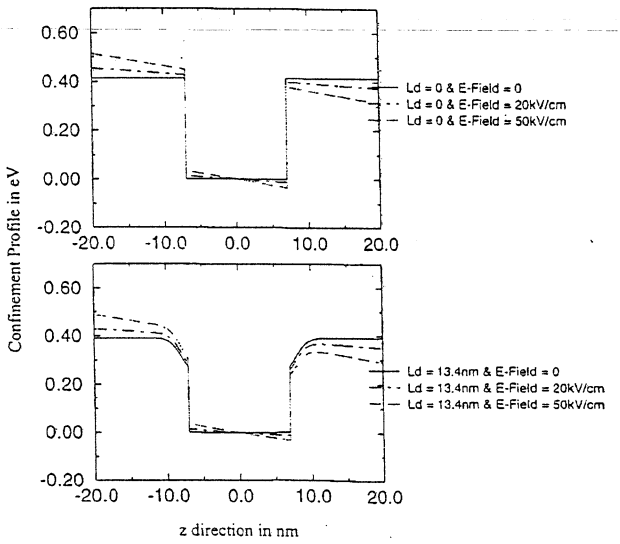

FIG. 3. The electron confinement profiles for as-grown (L_d=0 nm) and interdiffused samples (L_d=13.4 nm) and fields of 0, 20, and 50 kV/cm for a well width of 15 nm.

interdiffusion of the QWs, the square confinement profile is first changed to nonsquare confinement profile with L_d =0 nm [Fig. 3(a)]. The confinement profile is changed to nonlinear in shape with L_d=13.4 nm [Fig. 3(b)]. This leads to the decreasing of QW depth. It can also be seen that the disordered QW can also produce an asymmetric, nonlinear confinement profile due to the lowering of the barrier on one side with applied electric field.

Figure 4 shows the effect of the electric field on the electron and heavy hole ground state wave functions for L_d =0. The field induced shift of the electron eigenfunction to the right and that of the heavy hole eigenfunction, together with the increased penetration of the wave functions out of the well, are clearly evident. Thus, in the presence of an electric field, the overlap integral between the electron and heavy hole wave functions is reduced. For instance, its square shape from values around 0.98 in the absence of any field decreases drastically to around 0.34 when a field of 50 kV/cm is applied.

C. Quantum confined Stark shift

The exciton binding energy decreases with increasing applied field strength in all cases. The applied field causes

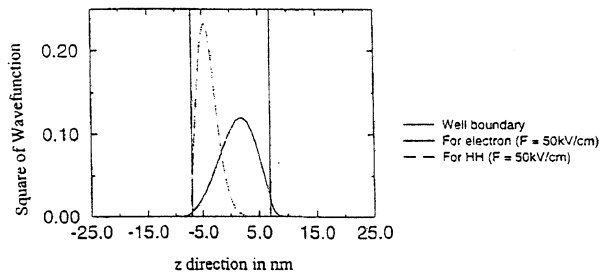

FIG. 4. Square of the wave function of E and HH in a QW structure with a 15 nm wide well.

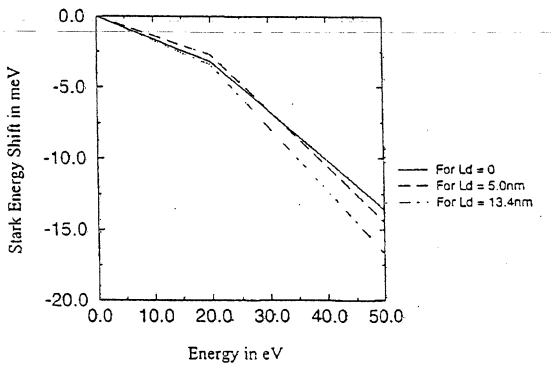

FIG. 5. The variation of the Stark shift energy for L_d of 0, 5, and 13.4 nm.

the electrons and heavy holes to move to the opposite sides of the well, which makes the exciton less two dimensional, thereby reducing the binding energy. In the initial stages of interdiffusion, the exciton binding energy shift decreases slightly followed by an increase to a value larger than the as-grown case. This reflects that there exists a changing effective width of the confinement profile, modified by the interdiffusion induced strain and applied field experienced by the electron and HH ground states.

The variation of the exciton Stark shift energy for the HH related transitions with applied electric field for various values of L_d are shown in Fig. 5. This Stark shift is much larger in magnitude than the exciton binding energy shift, indicating that the major contribution to the Stark shift comes from the ground state ($C1-HH1$) transition energy. As for small diffusion lengths and applied fields, the Stark shift is lower than that of the as-grown structure, while for the rest of the cases the Stark shift is greater in the interdiffused structure than in the as-grown structure. These results show that for a sufficiently large value of L_d, the exciton Stark shift in the disordered QW is greater than in the as-grown structure, implying that the applied field lowers the ground state subbands, and thus the band-gap transition energy, to a greater extent in the case of interdiffused QW in comparison to the as-grown structure.

D. Electroabsorption

The absorption coefficient spectrum is a function of the number and strength of the allowed transitions, and of the individual contributions of the HH and LH transitions to the two polarizations. This gives rise to the structure in Figs. 6(a) and 6(b). It can be seen that the TM absorption coefficient spectra contain less structure. Since the contributions of the HH transition to the TM polarization are much less profound, the LH subbands dominate the transition due to the optical selection rules.

From the room temperature absorption coefficient spectra, the exciton peak shifts to the lower energy with increasing applied field, indicating that the quantum-confined Stark effect takes place. At the same time, it decreases in value because the applied field pulls apart the electron and HH wave functions, reducing the overlap integral of electron–hole wave function. The exciton peak and the overall absorp-

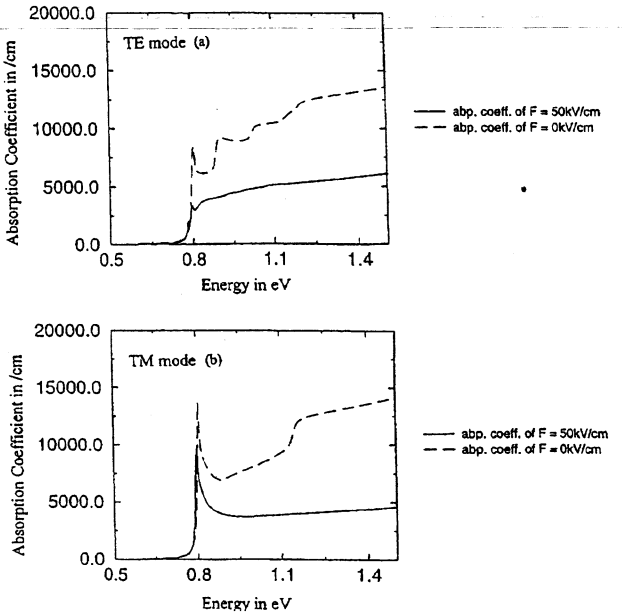

FIG. 6. The QW spectral absorption coefficients for: (a) TE and (b) TM polarizations for applied fields of 0 and 50 kV/cm with $L_d = 13.4$ nm.

tion coefficient are reduced at the same time because the overlap integral is one of the factors affecting the absorption coefficient. The decrease in the exciton peak for similar values of applied field is larger for the interdiffused QW than

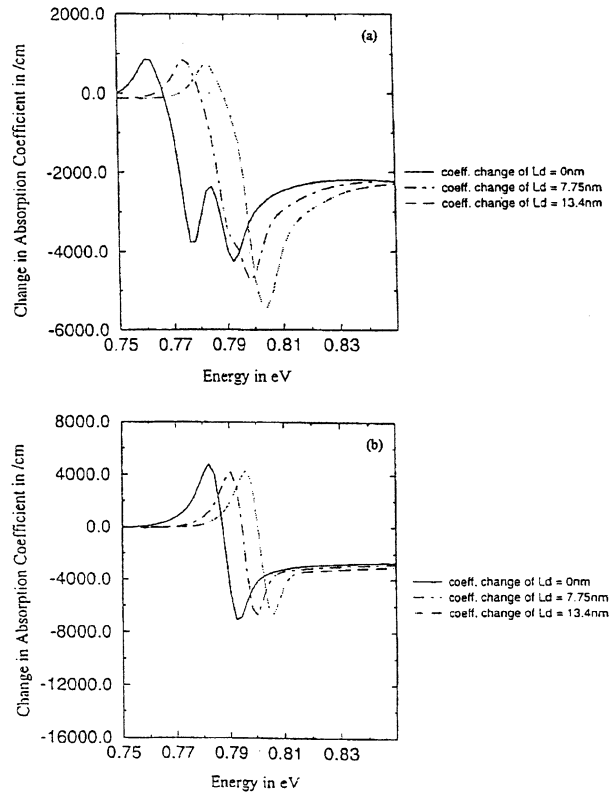

FIG. 7. The change in spectral absorption coefficient for: (a) TE and (b) TM polarizations for an applied field of 50 kV/cm and $L_d = 0$, 7.75, and 13.4 nm.

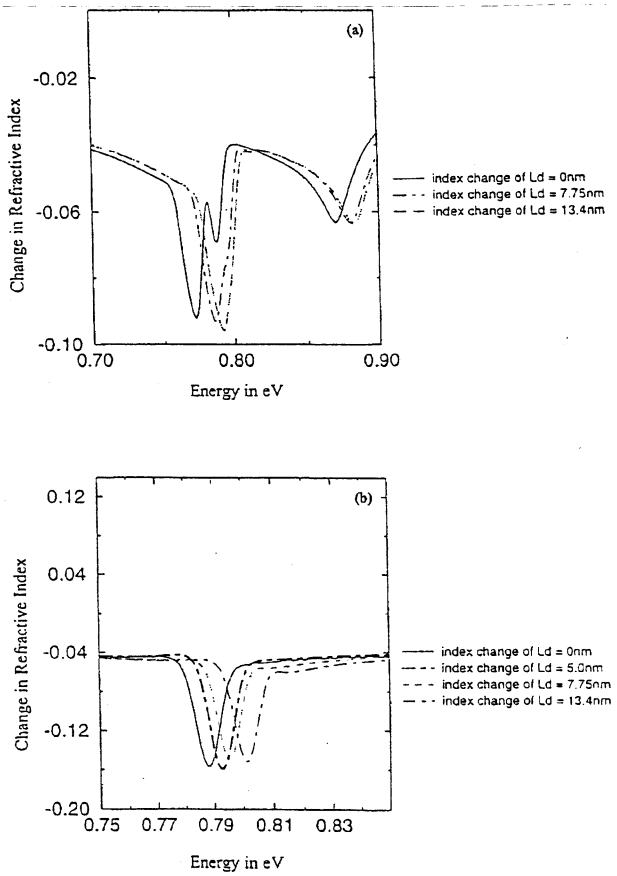

FIG. 8. The change in refractive index spectra for: (a) TE and (b) TM polarizations with an applied field of 50 kV/cm and $L_d = 0$, 7.75, and 13.4 nm.

for the as-grown QW. In the interdiffused QW, the electron and hole wave functions are less confined, resulting in a larger penetration out of the well while the electric field pulls apart the two wave functions. Consequently, the electron–hole wave function overlap, and thus the exciton peak, is reduced to a greater extent.

An improvement of the electroabsorption can be achieved with a larger L_d for the TE mode with applied field 50 kV/cm. The change of absorption coefficient with $L_d = 13.4$ nm is increased by 25% as compared with $L_d = 0$ nm, as shown in Fig. 7(a). This implies that the absolute maximum change in absorption coefficient can be achieved in InGaAs/InP interdiffused structure because of a weaker confinement. This enhancement gives an improved on/off ratio for the same waveguide modulator length or a reduced device length for the same on/off ratio, the latter being particularly attractive for high speed optoelectronic applications. As for the TM mode, the same change in absorption coefficient with increasing L_d except a shift of the spectrum as shown in Fig. 7(b). This is due to the fact that HH (which dominates the TE transition) is more sensitive to the field induced well shape change as it is closer to the bottom of the well.

E. Change in refractive index

Spectra of the change in refractive index are shown in Figs. 8(a) and 8(b). As for spectra with the same electric field applied but with different diffusion lengths, the change is a little larger when diffusion length increases. During the interdiffusion, the compositional profile and the consequent strain modification result in an increase of the ground state transition energy. A shift in the n_r spectrum is obtained when a higher field is applied. The transition energy decreases and the "blueshift" phenomenon is observed. These results demonstrate that using a field of** kV/cm Δn_r remains constant although its maximum is blueshifted. This implies that such an electro-optic modulator can be tuned to operate at different wavelengths, while the other device characteristics are retained.

IV. CONCLUSION

In this article, the effects of the electric field on the optical parameters of $In_{0.53}Ga_{0.47}As/InP$ diffused QWs have been modeled to provide an insight into the use of interdiffusion QWs to tune the characteristics of electro-optic modulators for a range of applications centered around a wavelength of 1.55 μm. The results show that using only group V interdiffusion, an enhanced QW electroabsorption can be achieved for the TE polarization, while for the TM, there are no significant changes that can be recognized with the exception of the blueshift of the spectrum. Both of these effects are subject to a small or zero change of electro-optic effect, that is very small modulation chirping. These effects are of mass importance for the application of optical modulators operating around 1.55 μm.

ACKNOWLEDGMENTS

This work is supported by the Research Grant Council earmarked grant of Hong Kong and the CRCG research grant of the University of Hong Kong.

[1] U. Koren, T. L. Koch, H. Presting, and B. I. Miller, Appl. Phys. Lett. **50**, 368 (1987).
[2] H. Temkin, M. B. Panish, and R. A. Logan, Appl. Phys. Lett. **47**, 978 (1985).
[3] R. J. Deri, E. Kapon, R. Bhat, M. Seto, and K. Kash, Appl. Phys. Lett. **54**, 1737 (1989).
[4] H. Temkin, T. Tanbun-Ek, and R. A. Logan, Appl. Phys. Lett. **56**, 1210 (1990).
[5] G. B. Stringfellow, *Organometallic Vapor-Phase Epitaxy-Theory and Practice* (Academic, New York, 1990).
[6] M. A. Herman and H. Sitter, *Molecular Beam Epitaxy-Fundamentals and Current Status*, Springer Series Materials Science, Vol. 7 (Springer, Berlin, 1989).
[7] E. H. Li, Mater. Res. Soc. Symp. Proc. **450**, 353 (1997).
[8] B. Tell, J. Shah, D. M. Thomas, K. F. Brown-Goebeler, A. DiGiovanni, B. I. Miller, and U. Koren, Appl. Phys. Lett. **54**, 1570 (1989).
[9] S. A. Schwarz, P. Mei, T. Venkatesen, R. Bhat, D. M. Hwang, C. L. Schwarz, M. Koza, L. Nazar, and B. J. Skromme, Appl. Phys. Lett. **53**, 1051 (1988).
[10] *Quantum Well Mixing and Optoelectronic Device Applications*, edited by E. H. Li, Milestone Series, Vol. 145, (Society for Photooptical Instrument Engineering, Bellingham, 1998).
[11] L. J. Guido, N. Holonyak, Jr., K. C. Hsieh, R. W. Kaliski, and W. E. Plano, J. Appl. Phys. **61**, 1372 (1987).
[12] T. Fujii, M. Sugawara, S. Yamazaki, and K. Nakajima, J. Cryst. Growth **105**, 348 (1990).
[13] M. D. Cameras, N. Holonyak, Jr., R. D. Burnham, W. Streifer, D. R. Scifres, T. L. Paoli, and C. Lindstron, J. Appl. Phys. **54**, 5637 (1983).
[14] K. Nakashima, Y. Kawaguchi, Y. Kawamura, H. Asahi, and Y. Imamura, J. Appl. Phys. **26**, L1620 (1987).
[15] H. Temkin, S. N. G. Chu, M. B. Panish, and R. A. Logan, Appl. Phys. Lett. **50**, 956 (1987).
[16] K. Mukai, M. Sugawara, and S. Yamazaki, J. Cryst. Growth **115**, 433 (1991).
[17] E. H. Li, J. Micallef, and W. C. Shiu, Mater. Res. Soc. Symp. Proc. **417**, 289 (1996).
[18] E. H. Li, K. S. Chan, B. L. Weiss, and J. Micallef, Appl. Phys. Lett. **63**, 533 (1993).
[19] E. S. Koteles, S. Charbonneau, P. Poole, J. J. He, M. Davis, M. Dion, G. Aers, and Y. Feng, Phys. Canada. **52**, 251 (1996).
[20] K. Mukai, M. Sugawara, and S. Yamazaki, Phys. Rev. B **50**, 2273 (1994).
[21] W. L. Bloss, J. Appl. Phys. **65**, 4789 (1989).
[22] J. F. Liang, Solid State Commun. **50**, 589 (1984).
[23] R. M. Cohen, J. Appl. Phys. **73**, 4903 (1993).
[24] J. Micallef, E. H. Li, and B. L. Weiss, Superlattices Microstruct. **13**, 125 (1993).
[25] D. J. BenDaniel and C. B. Duke, Phys. Rev. **152**, 683 (1966).
[26] E. H. Li and B. L. Weiss, Proc. SPIE **98**, 1675 (1992).
[27] H. C. Huang, S. Yee, and M. Soma, J. Appl. Phys. **67**, 2033 (1990).
[28] S. Adachi, J. Appl. Phys. **53**, 8775 (1982).
[29] E. S. Koteles, J. Appl. Phys. **73**, 8480 (1993).
[30] G. J. Shiau, C. P. Chao, P. E. Burrows, and S. R. Forrest, Appl. Phys. Lett. **65**, 892 (1994).